Atmos. Chem. Phys., 10, 1017–1030, 2010
www.atmos-chem-phys.net/10/1017/2010/

Atmospheric Chemistry and Physics

Vertical distribution of aerosols in the vicinity of Mexico City during MILAGRO-2006 Campaign

P. A. Lewandowski[1], W. E. Eichinger[1], H. Holder[2], J. Prueger[3], J. Wang[4], and L. I. Kleinman[4]

[1]IIHR-Hydroscience & Engineering University of Iowa, Iowa City, IA, USA
[2]Duke University, Rayleigh, NC, USA
[3]National Soil Tilth Laboratory, Ames, IA, USA
[4]Brookhaven National Laboratory, Upton, NY, USA

Received: 8 February 2009 – Published in Atmos. Chem. Phys. Discuss.: 11 March 2009
Revised: 20 October 2009 – Accepted: 16 November 2009 – Published: 1 February 2010

Abstract. On 7 March 2006, a mobile, ground-based, vertical pointing, elastic lidar system made a North-South transect through the Mexico City basin. Column averaged, aerosol size distribution (ASD) measurements were made on the ground concurrently with the lidar measurements. The ASD ground measurements allowed calculation of the column averaged mass extinction efficiency (MEE) for the lidar system (1064 nm). The value of column averaged MEE was combined with spatially resolved lidar extinction coefficients to produce total aerosol mass concentration estimates with the resolution of the lidar (1.5 m vertical spatial and 1 s temporal). Airborne ASD measurements from DOE G-1 aircraft made later in the day on 7 March 2006, allowed the evaluation of the assumptions of constant ASD with height and time used for estimating the column averaged MEE.

The results showed that the aerosol loading within the basin is about twice what is observed outside of the basin. The total aerosol base concentrations observed in the basin are of the order of 200 μg/m^3 and the base levels outside are of the order of 100 μg/m^3. The local heavy traffic events can introduce aerosol levels near the ground as high as 900 μg/m^3.

The article presents the methodology for estimating aerosol mass concentration from mobile, ground-based lidar measurements in combination with aerosol size distribution measurements. An uncertainty analysis of the methodology is also presented.

Correspondence to: P. A. Lewandowski
(piotr-lewandowski@uiowa.edu)

1 Introduction

1.1 MILAGRO 2006 Campaign

Mexico City Metropolitan Area (MCMA) is one of the largest and fastest growing populated areas in the world. With a population close to 20 million people and over 4 million vehicles, it is also the largest source of anthropogenic pollution in the region (CAM 2002, 2006). Its elevated location (∼2200 m) and tropical climate facilitate photolysis and transport of urban and industrial pollutants on a continuum of scales, from local, through regional, to continental. The chemical properties of MCMA pollutants have been analyzed in the past, e.g. MCMA-2003 campaign (Molina et al., 2007). The key results from the MCMA-2003 campaign formed the basis for yet a more extensive atmospheric measurement campaign MCMA2006/MAX-Mex/MIRAGE/INTEX-B, which was conducted in March 2006 in Mexico (Molina et al., 2008). Numerous chemistry studies have been carried out during the MILAGRO campaign (e.g. Stephens et al., 2008; Adachi and Buseck, 2008; Thornhill et al., 2008; DeCarlo et al., 2008; Nunnermacker et al., 2008; Kleinman et al., 2008; Talbot et al., 2008; Shon et al., 2008; Zheng et al., 2008; Doran et al., 2008). These studies revealed the significance of primary and secondary aerosols in the context of pollutant chemistry and air quality.

Physical properties of aerosols were also of great importance during the MILAGRO campaign in 2006. Spatial and temporal measurements of aerosol distribution in the Mexico City region were intended to provide information on transport, dynamics and evolution of particles aloft. Each component of the campaign was carried out on a different spatial

scale, from urban pollution supported by ground-based point measurements, to regional large scale pollution transport supported by wide-coverage aircraft measurements. The goal of the multiscale approach in the MILAGRO campaign was to bridge various points of the continuum to better understand the environmental impacts of pollution sources, such as MCMA. For that purpose several profilers, radiosondes and lidars (airborne, ground stationary and ground mobile) were dedicated to measuring the vertical layering of aerosols on different scales (Shaw et al., 2007).

1.2 Significance of lidar measurements

Lidars are particularly suitable for measuring physical properties of small particles. They capture the spatio-temporal distribution and mechanical mixing of particles suspended in the air (Eichinger et al., 2010a, b; Kao et al., 2002; Holmen et al., 1998) as well as mark the planetary boundary layer (PBL) height (Cooper et al., 2010; Davis et al., 2000; Eichinger et al., 2005; Cooper and Eichinger, 1994).

The University of Iowa mobile, ground-based, upward-looking lidar was used to support vertical measurements of aerosols on local and regional scales during the MILAGRO campaign. The 1064 nm lidar system was mounted on a flatbed truck and was able to make vertical measurements while in motion (Fig. 1). The lidar data was supported by coincident ground-based solar transmittance data, measured with an optical sun photometer. The solar photometer measured direct and indirect (almucantar) radiation once every 1–2 h (the measurements took about 8 min). These measurements enabled calculation of the column average aerosol size distribution (ASD) (Nakajima et al., 1996). Due to the nature of the measurements, (the propagating medium was the entire atmosphere), the ASD obtained from these measurements represents an average aerosol size distribution in the atmospheric column. To verify and evaluate the assumption of averaged constant ASD in the column, the airborne ASD data from DOE G-1 aircraft were analyzed with respect to altitude (Kleinman et al., 2008, 2009).

On 7 March 2006, in the presence of light, northerly winds (de Foy et al., 2008; Fast et al., 2007), the University of Iowa mobile vertical lidar system performed a North-South transect through the Mexico City basin. The lidar system measured the vertical and horizontal distribution of the various aerosol layers. The unique topography of the basin created conditions in which the northerly winds were venting the valley, mostly through a narrow pass in the south of the basin. The measurements on 7 March 2006, were intended to quantitatively capture the vertical and horizontal distribution of aerosols and observe the transition between the inside and the outside of the Mexico City basin. The exact route is illustrated in Fig. 2. The ground mobile lidar measurement effort was also intended to be coordinated with the airborne measurements carried out from the Veracruz airport. In retrospect, this effort was only somewhat successful due to traffic,

Fig. 1. The University of Iowa mobile vertical lidar (1064 nm 50 Hz 25 mJ/pulse laser, 100 MHz digitizer, 1.5 m spatial and 1 s temporal resolution) during the MILAGRO 2006 campaign.

different timing and location. Figure 2 also presents the path of DOE G-1 aircraft transect made shortly after the ground mobile lidar transect.

The University of Iowa mobile vertical lidar system performed measurements on other days as well. These included an East-to-West transect north of Mexico City, and two trips to/from Pachuca to Veracruz. The 7 March transect was the single most complete sun photometer and lidar dataset, and the only transect through Mexico City. Also the measurements from the second half of the month of March 2006 were often obscured by low level clouds (multiple Norte events described by de Foy et al., 2008; Fast et al., 2007), which complicated the data analysis and interpretation.

In all instances of this article, the time is reported as a local time in Mexico (not daylight savings time). The conversion between the local time (LT) used for the experiment and UTC is LT=UTC−6 h.

1.3 Mass Extinction Efficiency (MEE) approach

From an electromagnetic point of view, extinction efficiency is a measure of the amount of energy removed by a particle from a wave by means of scattering and absorption. Depending on the size of the particle, refractive index, and the wavelength of an incident radiation, Rayleigh and Mie theories report the exact values of the extinction efficiencies for spherical particles (such as the function presented in Fig. 3). Combining particles of all sizes in a medium with the corresponding extinction efficiencies, multiplied by their cross sectional areas, will result in the extinction coefficient (van de Hulst, 1957). The extinction coefficient is a macroscopic quantity describing the fraction of energy removed from an electromagnetic wave per unit distance for any given wavelength. Lidar measurements can provide spatially resolved

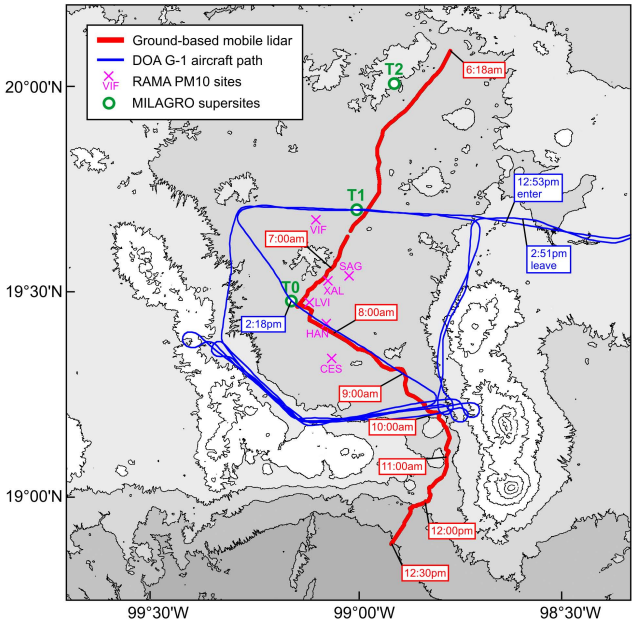

Fig. 2. The Mexico City basin. The red line indicates the mobile lidar trajectory with the corresponding time marks on 7 March 2006. The blue line represents the path of the DOE G-1 aircraft with corresponding time marks on 7 March 2006. The crosses depict selected RAMA PM_{10} sites and circles indicate MILAGRO supersites T0, T1 and T2.

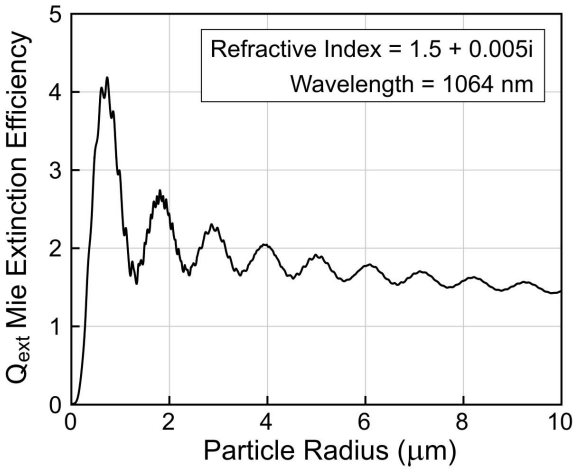

Fig. 3. Q_{ext} Mie extinction efficiency used for MEE calculations.

extinction coefficient data for the wavelength used in the lidar (Klett, 1981, 1985; Kovalev, 2003; Kovalev and Eichinger, 2004). Using the extinction coefficient data from the lidar and aerosol size distribution data from the sun photometer, one can invert the problem and determine the number (or mass) concentration of particles in the medium.

Extinction efficiency for 1064 nm implied from Mie theory (Fig. 3) is combined with column averaged ASD obtained from the sun photometer (Fig. 4b), resulting in a quantity called the Mass Extinction Efficiency (MEE). The MEE is a ratio of the total column extinction coefficient at the wavelength of the lidar, to the total mass concentration of aerosol in the column (Eq. 4). In electromagnetic sense, the MEE is a measure of the amount of energy removed from the wave by a specific aerosol (characterized by ASD) per unit length per unit concentration of the aerosol.

The MEE approach allows estimation of the absolute aerosol mass concentration with the resolution of lidar (1.5 m spatial and 1s temporal). This method is unique and introduces new data-rich capabilities to the aerosol research community. Due to the large spatial extent of the data, it is rather difficult to validate the MEE-derived results by means of in-situ measurements. Yet the effort of comparing this method with ground-based PM_{10} network in Mexico City is also presented in the results section.

2 Instruments

2.1 Lidar

Lidar operates by emitting a pulse of infrared laser light into the atmosphere. Particulates interact with the pulse and scatter light back to the lidar. The term "elastic" refers to scattering in which no energy is lost by the photons, so that the detected light is at the same wavelength as the emitted light.

For the purpose of the study, the University of Iowa lidar (Eichinger et al., 1999) was retrofitted into a mobile laboratory mounted on the bed of a truck (Fig. 1). The lidar operated continuously while the truck was in motion, simultaneously recording the GPS position of the instrument.

A Nd:YAG laser operating at the 1064 nm wavelength provided the light source. The laser was attached to a 0.25 m, f/10, Cassegrain telescope. The laser pulsed at 50 Hz with ∼25 mJ energy per pulse. The laser beam was emitted coaxial with the telescope. The backscattered signal was measured by an IR-enhanced Si-APD detector and then digitized by a 100 MHz digitizer. The resulting spatial (vertical) resolution was 1.5 m. The maximum useful range was 3400 m. For improved data accuracy, the signals from 50 pulses were averaged to 1 s profiles.

2.2 Sun photometer

A commercial, fully automated, Prede POM-01L sun photometer was used for this study. It was a 7 wavelength system with 315, 400, 500, 675, 870, 940 and 1020 nm filters operated by a filter wheel. The half-angle view of the instrument was 1 degree and the half-power bandwidth was 10 nm (with the exception of 3 nm for 315 nm). The instrument was mounted on top of the mobile laboratory only for the time of the measurement and taken down during travel. The measurements were taken while the vehicle stopped for

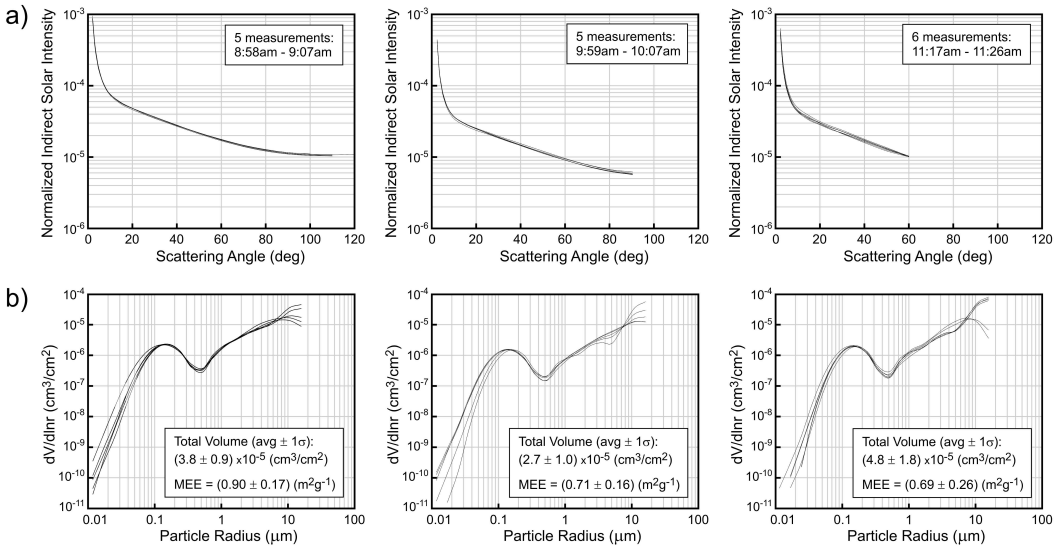

Fig. 4. The sun photometer measurements. **(a)** sun photometer raw data (showing 500 nm only) recorded in Mexico City on 7 March 2006, **(b)** corresponding aerosol size distributions (ASD) retrieved from the sun photometer measurements using SKYRAD.pack.v.4.2 inversion code. The inset shows the total volume and MEE values.

the measurements. It took about 8 min for the sun photometer to take a suite of 5 measurement sessions.

The instrument measured the relative radiation intensities (direct and almucantar) and was calibrated using a standard Langley method (Holben et al., 1998). The direct solar measurements provided total optical depth estimate and the almucantar measurements data were processed for aerosol size distribution using SKYRAD.pack v.4.2 (Nakajima et al., 1996).

2.3 ASD airborne measurements from DOE G-1 aircraft

The G-1 was equipped with instruments to measure chemical and microphysical properties of aerosol particles as well as gases that are either aerosol precursors or tracers of emission sources. Flight time was concentrated on characterizing fresh emissions over Mexico City and determining their evolution over time durations of order 1 day or less and spatial scales of order 100 km or less. For the above reasons, the ground lidar and the airborne ASD measurements do not coincide in time (the time separation on 7 March 2006, in the Mexico City basin was 5 h). The data obtained[1] from G-1 is useful for the purpose of validating the assumption of constant ASD in the column. The G-1 ASD data, used in this study, have a time resolution of 1 min. Trace aerosol properties are reported at ambient temperature and pressure. Local times are used in this study.

The aerosol inlet has a 50% cutoff at 1.5 μm (Brechtel, 2003) and is not a limiting factor for the instrumentation used in this study. Particle sizes between 0.1 and 3 μm were measured using a PCASP-100X (Particle Measuring Systems, Inc., Boulder, CO) with SPP-200 electronics (Droplet Measurement Technologies, Boulder, CO) mounted on an external pylon. The number distribution of particles over the size range 16 to 444 nm was determined using an SMPS consisting of a cylindrical Differential Mobility Analyzer (TSI Inc., model 3081) and a condensation particle counter (TSI Inc., model 3010). SMPS data were analyzed using the inversion procedure described by Collins et al. (2002). Aerosol size distributions are obtained at a relative humidity below 25%. Air flow to the DMA passes through a Nafion dryer. In general, the atmosphere over the Mexico City plateau was very dry (average relative humidity=27%) and one would expect that particles would have little associated water even without active drying.

2.4 Ground PM_{10} measurements

The ground PM_{10} measurements were conducted by the Mexican government scientists within the RAMA network (Red Automática de Monitoreo Atmosférico). The network included 16 sites located throughout Mexico City that had PM_{10} capability. The PM_{10} measurements are based on the beta attenuation method. The RAMA's beta attenuation analyzers provide a 1 h average PM_{10} data. Figure 2 shows the locations of the 6 RAMA sites nearest to the lidar route.

[1]Data archive ftp://ftp.asd.bnl.gov/pub/ASP%20Field%20Programs/2006MAXMex/

3 Data analysis

3.1 Lidar inversion method

Elastic lidar cannot measure extinction coefficients directly. Instead, it measures a relative backscattered power $P(r)$ which can be inverted to estimate extinction. Equation (1) is the range corrected lidar equation (Kovalev and Eichinger, 2004)

$$P(R)R^2 = C_0\beta(R)\exp\left(-2\int_0^R \alpha\left(R'\right)dR'\right), \quad (1)$$

where R is the distance from the lidar to a given sampling volume, β is the backscatter coefficient, α is the extinction coefficient, $C_0 = P_0 Ac\tau/2$ is the lidar constant, A is the telescope aperture area, τ is the laser pulse length, c is the velocity of light and P_0 is the power transmitted by the laser. In order to invert the lidar equation, the extinction and backscatter coefficients are assumed to be related by a power law (Klett, 1981, 1985)

$$\beta(R) = B_0\alpha^k(R), \quad (2)$$

where k is a constant power equal to 1 and B_0 is a scaling factor (often called the lidar ratio). With the assumption from Eq. (2), one can now estimate the extinction using the Klett method (Klett, 1981; Krichbaumer and Werner, 1994)

$$\alpha(R) = \frac{P(R)R^2}{\frac{P(R_0)R_0^2}{\alpha_0} + 2\int_R^{R_0} P(R')R'^2dR'} \quad \left[\frac{1}{\mathrm{km}}\right], \quad (3)$$

where $\alpha_0 = \alpha(R_0)$ is an assumed extinction coefficient at a distance R_0. While there are other more complex algorithms for calculating extinction (Kovalev and Eichinger, 2004), the Klett method is a fully adequate approach for the purpose of this study. An uncertainty analysis of the inversion procedure is presented in Appendix A.

3.2 Aerosol mass concentration

Knowledge of the aerosol size distribution (ASD) is useful in combination with lidar data. It allows the estimation of the absolute aerosol mass loading in the atmosphere. Studies show that the extinction (e.g. estimated from the lidar returns) is highly correlated with PM_{10} and $PM_{2.5}$ aerosol concentrations (Del Gusta and Marini, 2000; Lagrosas et al., 2005; Husar and Falke, 1996; Di Girolamo et al., 1999). The quantity that relates extinction and mass is called Mass Extinction Efficiency (MEE) (Lagrosas et al., 2005). It is a ratio of the total extinction in the column to the total column mass concentration of aerosols for any given ASD and any given wavelength. MEE links extinction efficiency, derived from the Mie theory, with aerosol mass estimates and, in conjunction with lidar measurements, can provide high spatial resolution aerosol mass estimates.

The total extinction is simply a product of Mie extinction efficiency, the particle cross-sectional area and the number of particles of each size integrated over all particle sizes for a given wavelength (the numerator in Eq. 4). The total mass of aerosol is a product of the particle volume, the mass density of particle and the number of particles, integrated over all sizes (the denominator in Eq. 4). Equation (4) presents MEE in the following form (Lagrosas et al., 2005)

$$\mathrm{MEE} = \frac{\pi\int_{r_1}^{r_2} r^2 Q_{\mathrm{ext}}(r,\lambda,m)n(r)dr}{\frac{4}{3}\pi\rho\int_{r_1}^{r_2} r^3 n(r)dr} \quad \left[\frac{1/\mathrm{m}}{\mathrm{g/m^3}}\right], \quad (4)$$

where r is the particle size, r_1 and r_2 are ASD limits, Q_{ext} is Mie extinction efficiency calculated for the 1064 nm wavelength (Fig. 3), m is the assumed refractive index of the aerosol, $n(r)$ is a given ASD (Fig. 4b) and ρ is the particle density. Although $n(r)$ and Q_{ext} are functions of the altitude and the location (Q_{ext} indirectly through the refractive index), both are assumed constant for the analysis in this study. Spatially resolved measurements of ASD and refractive index are difficult, expensive and often require aircraft sampling for that purpose.

Using the extinction coefficient estimated from the lidar data, one can obtain aerosol mass concentrations with the resolution of the lidar measurements

$$C(R) = \frac{\alpha(R)}{\mathrm{MEE}} \quad \left[\frac{\mathrm{g}}{\mathrm{m^3}}\right], \quad (5)$$

where α and MEE have been previously defined. The entire data processing flow leading to Eq. (5) is shown in Fig. 5. Note that the concentration estimates in Eq. (5) are spatially resolved only due spatially resolved lidar data. The MEE in Eq. (5) is not spatially resolved.

4 Results and discussion

4.1 Aerosol size distribution

During the transect, 15 sun photometer measurements were taken in and outside the basin, in 3 discrete series (Fig. 4a). The data from the measurements were used to estimate the column averaged aerosol size distribution (ASD) with SKYRAD.pack.v.4.2 software[2] (Nakajima et al., 1996). The resulting ASD estimates are presented in Fig. 4b.

There were 3 sun photometer measurement sessions, which consisted of 5 individual sky radiance measurements in each session. The sun photometer measurement data, presented in Fig. 4a, are nearly identical with little deviation. Although the differences in raw data were small, they propagated into noticeable differences in the respective size distributions, total volume of aerosols and MEE values (Fig. 4b).

[2] Available at http://www.ccsr.u-tokyo.ac.jp/~clastr/

Of all the 3 sets of raw data (Fig. 4a), the earliest measurement (∼09h00) has the largest number of measured scattering angles due to the lowest sun elevation angle. This enabled better convergence of the inversion software and, thus, the earliest measurements show the least uncertainty in the ASD shape, total volume and the MEE value.

Despite the uncertainties, all of the 3 size distribution sets are similar in shape, which implies that the dominant source of particles in the column is common to all the measurements. The spectra are bimodal with the fine mode peaking at around 0.2 μm and the coarse mode with the peak at around 7–8 μm. The fine mode is consistent with the DOE G-1 aerosol data from DMA.

With the column averaged ASD estimates from the sun photometer, it is impossible to account for the varying composition of the urban plume (e.g. crustal, biogenic aerosols, etc.) because the photometer measurements represent the entire atmospheric column. As a consequence, the variations of the ASD due to surface level emissions are averaged over the entire atmospheric column and are indistinguishable from simple column transmittance measurements (like the one in Fig. 4b).

4.2 MEE results

MEE is sensitive to the shape of the ASD function. The literature reports MEE values for 355 nm, 532 nm, 550 nm, 580 nm, 723.37 nm ranging from 0.2 $m^2\,g^{-1}$ (coarse particles dominant) to 14 $m^2\,g^{-1}$ (fine particles dominant) (Dubinsky et al., 1985; Tang, 1996; Dillner et al., 2001; Mallet et al., 2003; Lagrosas et al., 2005). The literature does not report MEE values for 1064 nm.

The MEE estimated for 1064 nm from the ASDs in this study ranged from 0.5 $m^2\,g^{-1}$ to 1.3 $m^2\,g^{-1}$ (with the particle standard density, ρ, assumed 1 g/cm^3 for all the calculations). Higher values of MEE were observed inside the Mexico City basin whereas lower values were observed outside of the basin. To maintain continuity in the mass concentration calculations using the lidar data (Eq. 5), we assumed a constant ASD (and therefore a constant MEE) for the entire measurement period. This assumption is supported by DOE G-1 aerosol DMA measurements made at various altitudes (Fig. 8) which reflect a relatively small fluctuation of MEE with altitude (standard deviation of 7%).

The earliest sun photometer measurement set 08h58–09h07 was used for the entire data analysis. The choice of the ASD dataset is somewhat arbitrary, although the 08h58–09h07 ASD data yields the most consistent results from all the ASD measurements that day. The corresponding value of MEE for the 08h58–09h07 dataset was 0.90±0.17 $m^2\,g^{-1}$ and that value of MEE was used for the entire analysis.

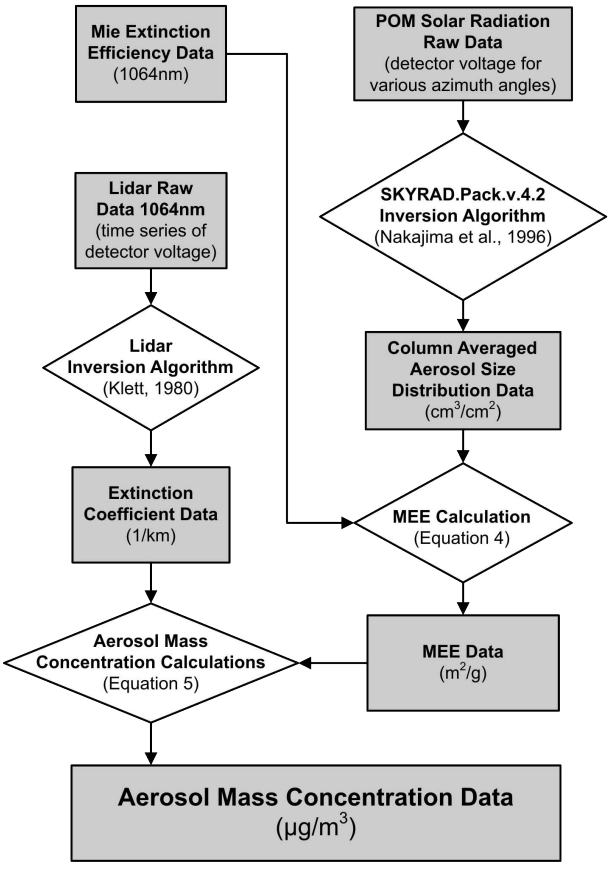

Fig. 5. Aerosol mass concentration data processing flowchart.

4.3 Aerosol size distribution from DOE G-1 aircraft

On 7 March 2006, the DOE G-1 aircraft measurements were conducted in the Mexico City basin with the main focus on the southern inner rim of the basin (blue line in Fig. 2). The airborne aerosol size distribution from DMA was measured in a 0.016–0.44 μm particle range at various altitudes. An example of an aerosol size distribution from the instrument is presented in Fig. 8a. The size distribution yields an accumulation mode at around 250–300 nm diameter (excellent agreement with the ASD data from the photometer with the peak around 150 nm radius) and a nucleation mode at 0.04–0.07 μm (not observed by the photometer). The nucleation mode is distinctly observed only at ground level which suggests the ground source emissions from the Mexico City basin. The course mode is not observed by the DMA.

The airborne aerosol size distribution data were used mainly to validate the assumption of a constant averaged aerosol size distribution from the photometer data. The airborne data was used to calculate the MEE at all available altitudes, as shown in Fig. 8b. Because the airborne aerosol size distribution data is measured only in the part of the size spectrum (0.016–0.44 μm), the value of MEE from airborne measurements (Fig. 8b) does not correspond to the value of MEE

obtained from the photometer measurements and, therefore, the results from these instruments cannot be directly compared.

The standard deviation of the MEE was calculated with respect to the altitude and served as a measure of the uncertainty for the assumption of the averaged aerosol size distribution in the column used in the analysis from the photometer. The standard deviation of the MEE across the column equals to 7%, which suggests that the variation of the aerosol size distribution has a rather small effect on the MEE analysis.

4.4 Transect through Mexico City

The meteorological conditions reported for 7 March 2006, were favourable with respect to the purpose of the study: persistent, light, northerly winds for the Mexico City basin, warm, mostly sunny, stable surface conditions in the morning. The balloon soundings from Mexico City airport reported for 12h00 UTC on 7 March 2006, indicate light E to N winds of 5 m/s between 780–600 mb and N to NW winds of 5–10 m/s between 600–500 mb (the height of the boundary would be observed). 7 March 2006, was a clear day. The clear sky allowed proper sky radiance measurements (not obscured by clouds). Clear skies were the prevailing conditions in the first half of March 2006. The second half of the month was generally less favourable for sky radiance measurements as the clouds were often forming in the sky. There were 3 separate Norte events in the second half of the month. The detailed description of the meteorological conditions during the campaign is included in de Foy et al. (2008) and Fast et al. (2007).

The transect through the Mexico City basin started at 06h18 on 7 March 2006, in the city of Pachuca, about 70 km NE of Mexico City (Fig. 2). The direction of the transect was north to south. Figure 6b shows lidar-derived total aerosol concentration cross section corresponding to Fig. 2. Figure 6 additionally presents the total aerosol concentrations extracted from the lidar at 200 m above the ground (Fig. 6c) and the total optical depth for the 1020 nm wavelength from the solar photometer (Fig. 6d).

The reason why the concentrations from the lidar were retrieved from 200 m above the ground in Fig. 6c and Fig. 7 is related to the dynamic range of the digitizer (12 bit ADC). The signal observed by the detector decreases with distance as $1/R^2$, so within the first 200 m the signal is huge compared to the signal at, for example, 2000 m. By disregarding the signal from the first 200 m, the maximum cap of the signal (governed by $1/R^2$) is brought down to lower values and, therefore, increased the dynamic resolution of the digitizer in the range of interest (500–3000 m). Ignoring the signal in the first few hundred metres is a common practice in lidar systems in which the laser beam is coaxial with the telescope. It is a trade-off between the minimal useful range and the dynamic resolution of the signal.

As mentioned earlier in the text, the lidar can measure as high as 3400 m above the ground. That means that, depending on the altitude of a location, the highest observable extinction coefficient related to the lidar measurement falls between 5000 and 6000 m m.s.l. One could argue that the total optical depth from the lidar at 1064 nm (vertically integrated extinction coefficient) shown in Fig. 6d is underestimated because it does not take into account the extinction above 6000 m m.s.l. to the top of the atmosphere. Rogers et al. (2009) have shown in multiple cases (10, 12, 15 March 2006) that AOD over Mexico City drops to 0 at around 4–4.5 km m.s.l. It means that the air above 4.5 km m.s.l. is clean and does not contribute significantly to the total optical depth associated with aerosols. It also means that the underestimation of the total optical depth measurements from the lidar (Fig. 6d) is expected to be small.

At the beginning of the lidar measurements, at around 06h20, the aerosol curtain graph indicates a residual layer at approximately 4500 m m.s.l. with high concentration values decaying with time. This effect is due, at least in part, to water condensation on the particulates. The water content data obtained from the 12h00 UTC balloon soundings from Mexico City confirms that hypothesis. The lifted condensation level (LCL) is found at around 4500 m m.s.l. in the balloon soundings. One of the potential explanations for the effect is the sun warming up the air after dawn. In such a case, the relative humidity decreases and the water evaporates from the particulates, resulting in the decrease of the apparent concentration values in time.

At around 06h30, about 10 km south of the starting point, the Mexico City plume is found at about 200–300 m above the ground as the lidar continues approaching the city, the plume is observed lower to the ground. At 07h00, the mobile lidar approached dense traffic congestion on a major highway going through Mexico City (Fig. 6a indicates slow velocities from a traffic jam and Fig. 6b represents an abrupt increase in concentrations). The congestion happened exactly in the mid-point between T1 and T0 supersites (Fig. 9). This event resulted in an outburst of ground aerosol concentrations due to emissions from the congested traffic conditions (peaking at $\sim 900\,\mu g/m^3$). While the concentration estimate seems to be extremely high, one should remember that this was an instantaneous measurement directly above a 6 lane highway. A high number of vehicles travelling on that road in either direction (diesel trucks and other petroleum vehicles with no or poor emission control) and the strength of the stable boundary layer at that early morning hour contributed to the sharp increases in particulate concentration. In addition to the exhaust emissions, vehicles also tend to pick up a large amount of road dust and inject it directly into the boundary layer. It is not unusual to see similar structures localized over major thoroughfares in scanning lidar images (Cooper and Eichinger, 1994; Eichinger and Kraye, 1998). The surface structures observed during that time of day rose to about 1 km in height but did not reach nor mix with the

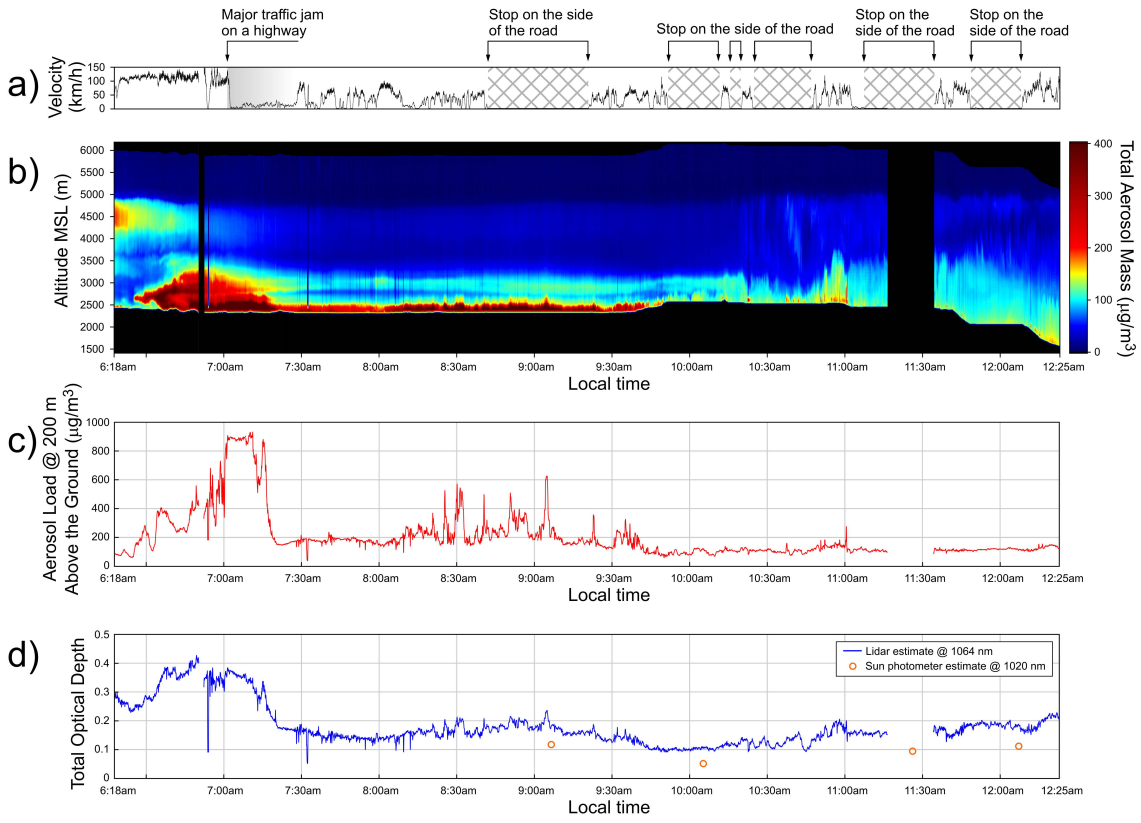

Fig. 6. Lidar vertical profiles of aerosol loadings over Mexico City on 7 March 2006: **(a)** lidar velocity over ground, indicating periods of heavy traffic and several stops, **(b)** colour-coded total aerosol vertical mass concentrations in Mexico City basin, **(c)** mass concentration levels at 200 m above the ground, **(d)** total optical depth calculated from lidar data (blue line) and from sun photometer (orange cirles).

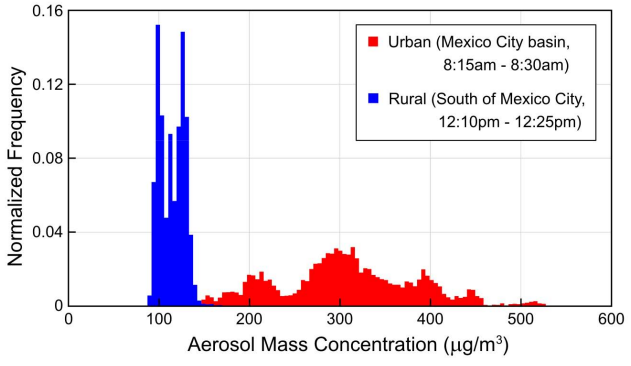

Fig. 7. A histogram of the aerosol mass concentration values observed at 200 m above the ground over a 15 min time-span, inside the city basin (red) and outside the basin (blue).

upper residual layer. At around 07h30, the traffic congestion decreased and the lidar proceeded further into the city. At this point, the height of the pollution plume was observed to be at around 200–300 m above the ground with base concentrations of about 200 μg/m^3. The values of the concentrations are similar to the RAMA network measurements, recording a similar average morning rush hour PM_{10} concentration level in the close by locations in the city (Fig. 9, XAL, VIF, CES, SAG, etc.).

From about 07h30, another layer appears at around 3000 m m.s.l. (500 m above the ground). The layer is separated and at this point does not mix with the pollution from the ground. These conditions remained constant throughout the city until the southern rim of the basin was reached at about 09h50. The southern outlet from the basin is about 200 m higher than the average elevation of the basin. In stable boundary conditions, the difference in elevation may act to keep the ground pollution from leaving the valley southbound. Although not enough evidence was collected to state that this conditions was observed on 7 March 2006.

Halfway through the pass (∼10h25), the vertical layering of the plume changed. The 3000 m m.s.l. layer disappeared while the 4500 m m.s.l. residual layer started to mix in with the rising boundary layer. The mixing as well as the fact that the lidar was moving out of the basin resulted in lower concentrations of around 100 μg/m^3 at ground level and higher concentrations across the boundary layer.

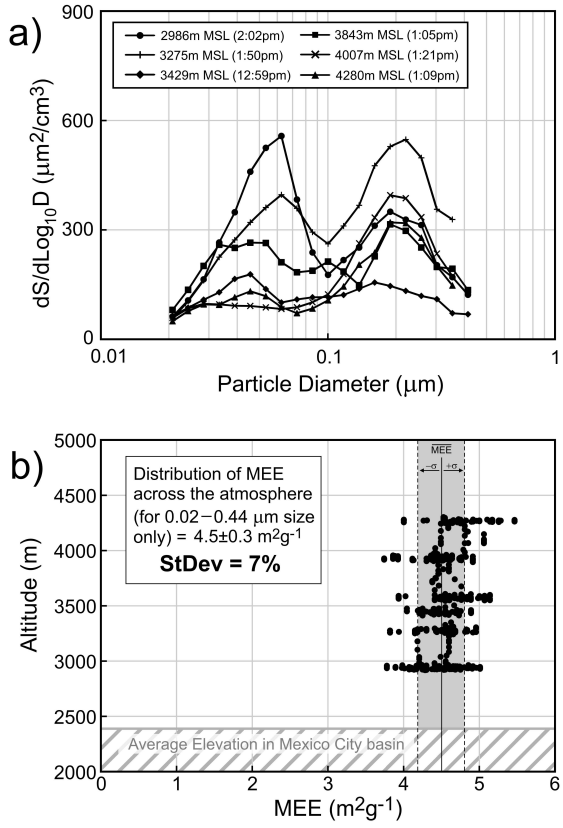

Fig. 8. The airborne aerosol size distribution (ASD) data from Differential Mobility Analyzer (DMA) from DOE G-1 aircraft observed on 7 March 2006 over Mexico City basin: **(a)** ASD at different altitudes, **(b)** the distribution of corresponding Mass Extinction Efficiency (MEE) with respect to altitude. Note that MEE was calculated for 0.02–0.45 μm aerosol sizes available from DMA, not for the entire aerosol size spectrum.

Vertical mixing intensified at around 11h00 where local ground pollution was lofted as high as 1 km above the ground and entrained with the high altitude residual layer. At around 11h35, the lidar began the descent outside of the valley. The local ground pollution continued to grow in height but did not mix with the high level (4500 m m.s.l.) residual layer. Both structures were separated by a thin stable layer of relatively clean air. These conditions were maintained until the end of the transect at 12h25.

Figure 7 shows a histogram of the lidar-derived total aerosol concentration estimates for the inside (urban) and outside (rural) areas of the Mexico City basin. The rural concentrations (blue) show a narrow mode with a centre located at around 110 μg/m^3. The urban concentrations are multimodal suggesting multiple contributors and pollution in the city. The values of the concentrations range from 150 μg/m^3 to 450 μg/m^3 with the most intensive mode at 300 μg/m^3.

Figure 10 presents the lidar data in 3-D display where each lidar profile is rendered with respect to its actual geographic location. The 3-D lidar data is overlaid onto a digital elevation model of the region using GIS software.

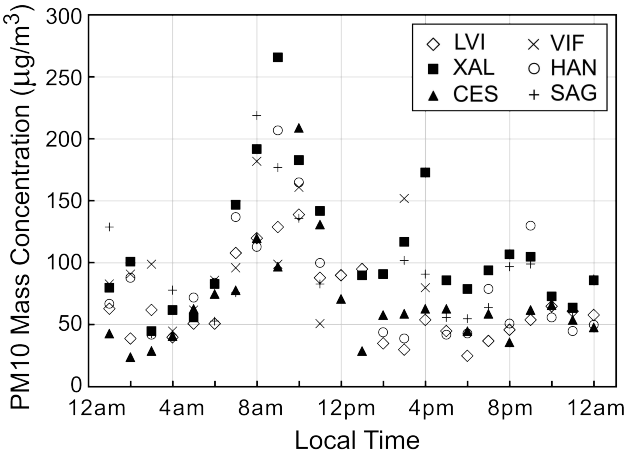

Fig. 9. Time series of aerosol PM_{10} concentrations for selected RAMA ground monitoring sites on 7 March 2006.

4.5 RAMA network

Figure 9 shows hourly-average PM_{10} concentrations with values between 100 and 250 μg/m^3 for times between 06h00 and 12h00. The values of the RAMA data are consistent with the aerosol mass concentrations observed with the lidar. The base average aerosol mass concentration in Mexico City estimated from the lidar was estimated at 200 μg/m^3 (Fig. 6c). Short, small scale events of higher aerosol mass concentration were also observed with the instantaneous lidar measurements within the basin (Fig. 6c). These events would not be distinctly visible in the RAMA network data because of the 1 h temporal resolution of the instruments in the network.

The data from the RAMA network and the data from the mobile measurements allow for only general comparisons. Note that RAMA network reports concentrations at ground level and the lidar concentrations are retrieved at 200 m above the ground. The RAMA network measures only particles smaller than 10 microns while bigger particles are not uncommon in dusty environment of Mexico City. The lidar MEE retrieved concentrations show the total loading with no distinction between fine and coarse particles.

4.6 Uncertainty analysis

This section estimates the uncertainties of the major components of the data analysis leading to aerosol mass concentration.

4.6.1 Uncertainty of extinction coefficient

The uncertainty related to the lidar estimates of the extinction coefficient can be approached through the analysis of

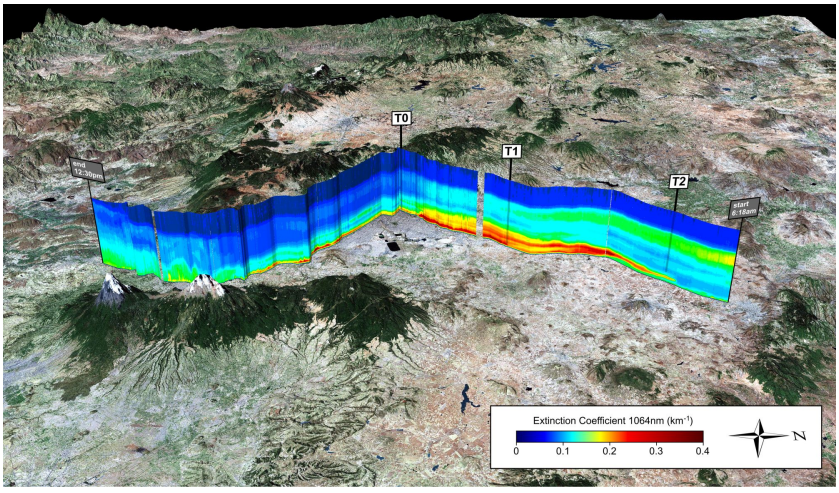

Fig. 10. The lidar colour-coded vertical distribution of aerosols over Mexico City basin on 7 March 2006, looking West. The dark red indicates heavy aerosol loading and dark blue indicate clean air in the free troposphere. The transect presents a stable layering within the valley and an intensive vertical mixing outside of the basin (elevation model and satellite imaging source: USGS).

the Klett's inversion algorithm (Eq. 3). There are 4 major sources of uncertainties related to the lidar inversion: (1) the uncertainties from the individual measurements at each range $P(R)R^2$, (2) the uncertainty of the integral in the denominator, (3) the uncertainty of the initial estimate of the far field extinction α_0 and (4) the uncertainty of the value of the lidar signal at the far range $P(R_0)R_0^2$. The detailed analysis of these lidar uncertainty components is presented in Appendix A. The overall uncertainty of the extinction coefficient from the lidar is estimated at 5%.

4.6.2 Uncertainty of MEE

Mass Extinction Efficiency is a complex quantity involving numerous assumptions, most importantly the use of column averaged aerosol size distribution and the stationarity of the distribution. This particular assumption was evaluated via airborne aerosol size distribution measurements from DOE G-1 aircraft made over Mexico City later on 7 March 2006. The ASD airborne data from DMA was used to calculate MEE as a function of altitude. The standard deviation of MEE with respect to altitude was used as a measure of the uncertainty associated with the assumption. The overall deviation of MEE with respect to altitude was 7%. Note that MEE calculated from the DMA covered the submicron part of the size spectrum (0.016–0.44 μm) so that the value of MEE from the DMA cannot be compared to the value of MEE obtained from the photometer. The MEE data from DMA was used solely for the determination of the uncertainty associated with the MEE calculations from the photometer.

Other sources of the uncertainty of MEE calculated from the photometer are related to the aerosol inversion algorithm. The inherent assumptions in the inversion algorithm include the refractive index, shape of the particles, meteorological conditions, etc. The uncertainty of the algorithm is typically of the order of 15–25% (Nakajima et al., 1996; Dubovik et al., 2000).

Another source of the uncertainty in MEE analysis is the particle density. The particle density measurement is a separate subject of its own. An extensive discussion on various density measurements and their uncertainties can be found in the literature (Kleinman et al., 2008, 2009; DeCarlo et al., 2004; Emets et al., 1992; Kelly and McMurry, 1992; Le Bronec et al., 1999). The standard particle density (1 g/cm^3) was arbitrarily used for the study with 30% uncertainty.

4.6.3 Uncertainty of aerosol mass concentration

Equation (6) incorporates all the above mentioned uncertainties related to the data processing leading to the assessment of the aerosol mass concentration. The measure of relative uncertainty of aerosol mass concentrations from MEE and lidar-estimated extinction coefficient are assumed to be statistically independent and can be added in quadrature

$$\frac{\delta C}{C} = \sqrt{\left(\frac{\delta\alpha_{\mathrm{LIDAR}}}{\alpha_{\mathrm{LIDAR}}}\right)^2+\left(\frac{\delta n_{\mathrm{COLMN\_AVG}}(r)}{n_{\mathrm{COLMN\_AVG}}(r)}\right)^2+\left(\frac{\delta n_{\mathrm{INVER}}(r)}{n_{\mathrm{INVER}}(r)}\right)^2+\left(\frac{\delta\rho_{\mathrm{PART}}}{\rho_{\mathrm{PART}}}\right)^2} = \sqrt{0.05^2+0.07^2+0.2^2+0.3^2} = 37\% \quad (6)$$

where δ denotes the uncertainty of a given quantity. The resulting value of uncertainty of the aerosol mass concentration estimates is 37%.

There are a number of sources of uncertainties that are not accounted for in this analysis. One example of a source of uncertainty is the fact that the lidar took the measurements

directly above the roads. It was shown before that the cars are not only the source of fine aerosols due to gas burning but are also a separate source of mechanical mixing of the road dust that is lofted high above the roadways (e.g. Eichinger et al., 1993). Scanning lidar measurements in urban areas show dramatically increased particulate concentrations above major thoroughfares, though this source of uncertainty is difficult to evaluate.

From the theoretical point of view, the MEE is based on an entirely correct physical approach. Although the results contain uncertainties, the data set can be beneficial for any large scale aerosol data modelling. We believe that the strengths of the MEE combined with lidar data outweigh the limitations of this approach and open totally new lidar capabilities for the community.

5 Conclusions

The study presents the horizontal and the vertical distribution of aerosols over Mexico City basin for 7 March 2006. Early in the morning on that day, the particular matter contained within the boundary layer was observed as high as 1500 m above the ground in Mexico City. The high levels of aerosols associated with heavy traffic (and traffic jams) events indicate that the transportation system in Mexico City plays an important role in facilitating aerosol loadings in the city basin boundary layer.

The total aerosol mass concentration base levels in the basin are of the order of 200 μg/m^3 with small scale events peaking as high as 900 μg/m^3. The concentrations outside of the basin (on the southern side of the rim) are about half of what was observed within the basin with base values of 100 μg/m^3. The vertical mixing outside of the basin is much more evident, with mixing depth as high as 2000 m above the ground. The residual layer is distinctly separated from the ground-based mixing. The findings presented in the article are based only on one transect.

The airborne ASD data from DOE G-1 shows 7% standard deviation with altitude. The uncertainty related to the lidar inversion is estimated at 5%. The uncertainty related to ASD inversion from the photometer and the particle density is assumed at 20% and 30%, respectively. The overall uncertainty of the aerosol mass concentration from MEE analysis is evaluated at 37%.

In the future, the quantitative estimation of the total aerosol loads from the mobile lidar could be improved by continuous measurements of the aerosol size distribution along the measurement route as well as having more accurate particle density measurements. Using secondary roads for transects could potentially reduce the effect of the major thoroughfares, which can greatly set off the overall aerosol contributions from the urban areas.

Appendix A

The uncertainty of the lidar inversion

Klett's lidar inversion algorithm

$$\alpha(R) = \frac{P(R)R^2}{\frac{P(R_0)R_0^2}{\alpha_0} + 2\int_R^{R_0} P(R')R'^2 dR'} \quad \left[\frac{1}{\text{km}}\right] \tag{A1}$$

contains 4 major sources of uncertainty which propagate to the extinction coefficient $\alpha(R)$.

The first source is the average fractional uncertainty of the range corrected lidar measurement, $P(R)R^2$ in the numerator. This uncertainty is related to the signal-to-noise ratio of the system and is evaluated at the average range, R_{AVG}. The nature of the lidar measurements implies that this uncertainty tends to be smaller closer to the lidar and greater further away from the lidar. The square root mean noise level is less than 10 mV out of approximately 400 mV at a range of 1500 m, with closer ranges having less uncertainty and longer ranges having more. The uncertainty from this source is estimated on average at 3%

$$\frac{\delta\alpha_1}{\alpha} = \frac{\delta P(R)R^2}{P(R_{\text{AVG}})R_{\text{AVG}}^2} \approx 3\%. \tag{A2}$$

The second source of uncertainty in the lidar inversion is related to the uncertainty of the integral in the denominator, which is a function of how many lidar measurements are summed. For an atmosphere that is polluted, but not turbid, the integral in the denominator in Eq. (A1) usually does not dominate the first term in the denominator, but is comparable in magnitude. For simplicity of the estimate, we assume the terms are approximately equal $\frac{P(R_0)R_0^2}{\alpha_0} \approx \int_{R_0}^{R} P\left(R_0'\right)R_0^{2\prime}dR'$. If we assume that the errors in each of the lidar values are statistically independent, then the uncertainty is related to the number of data samples, N, used for the integration which was well over 1000 for this study. The uncertainty associated with this source is estimated at about 2%

$$\frac{\delta\alpha_2}{\alpha} = \frac{\delta\left(\int_{R_0}^{R} P\left(R'\right)R^2 dR'\right)}{\frac{P(R_0)R_0^2}{\alpha_0} + \int_{R_0}^{R} P(R')R^{2\prime}dR'} \approx \frac{\sqrt{N}}{2N} = 2\%. \tag{A3}$$

The third source of uncertainty in the inversion is linked to the value of the known extinction coefficient, α_0, at the distance R_0. In this study, we have assumed that the atmosphere is particulate-free at altitudes just under 6 km m.s.l., so that the assumed extinction is molecular only. This is not a bad assumption considering the data from the airborne measurements over Mexico City presented in Rogers et al. (2009). As there are certainly particles at the higher altitudes, we estimate the uncertainty of the assumption of α_0 at 5%. Again

we note that the two terms in the denominator are of comparable size. This leads to an uncertainty in the extracted extinction coefficient of about 2.5%

$$\frac{\delta\alpha_3}{\alpha} = \frac{\frac{\delta\alpha_0}{\alpha_0}\left(\frac{P(R_0)R_0^2}{\alpha_0}\right)}{\frac{P(R_0)R_0^2}{\alpha_0} + \int_{R_0}^{R} P(R')R^{2\prime}dR'} \approx \frac{1}{2}\frac{\delta\alpha_0}{\alpha_0} = 2.5\%. \quad \text{(A4)}$$

The fourth lidar inversion-related source is the uncertainty of the actual value of the range corrected lidar signal at the location of the estimated extinction, α_0 which is $P(R_0)R_0^2$. The uncertainty of the signal in far range is estimated to be 5%, which results in a 2.5% contribution in the extracted extinction coefficients

$$\frac{\delta\alpha_4}{\alpha} = \frac{\frac{\delta P(R_0)R_0^2}{\alpha_0}}{\frac{P(R_0)R_0^2}{\alpha_0} + \int_{R_0}^{R} P(R')R^{2\prime}dR'} \approx \frac{1}{2}\frac{\delta P(R_0)R_0^2}{P(R_0)R_0^2} = 2.5\%. \quad \text{(A5)}$$

Combining the above inversion uncertainties in quadrature results in 5% overall uncertainty (assuming independence of the sources of error). This value is unusually small and is due to the particular conditions. Most of the contributing data in Mexico City (pollution) was located near closer to the lidar where the accuracy of the measurement is high and allows a higher quality estimate of the far range extinction coefficient α_0 in the free troposphere.

$$\frac{\delta\alpha_{\mathrm{LIDAR}}}{\alpha} = \sqrt{\left(\frac{\delta\alpha_1}{\alpha}\right)^2 + \left(\frac{\delta\alpha_2}{\alpha}\right)^2 + \left(\frac{\delta\alpha_3}{\alpha}\right)^2 + \left(\frac{\delta\alpha_4}{\alpha}\right)^2} \approx 5\% \quad \text{(A6)}$$

There is another implicit assumption in the lidar inversion that is not accounted for in this analysis. The particle size distribution and the aerosol properties are assumed to be homogenous throughout the depth of the atmosphere so that the extinction to backscatter ratio can be assumed to be constant throughout the depth of the measured atmosphere. Evaluation of the effect of this assumption is difficult in that it is impossible to know how much the aerosol properties change with altitude, and even if they were known, there are no analytical tools at this point to estimate the effect of the changes on the inversion.

Edited by: L. Molina

References

Adachi, K. and Buseck, P. R.: Internally mixed soot, sulfates, and organic matter in aerosol particles from Mexico City, Atmos. Chem. Phys., 8, 6469–6481, 2008, http://www.atmos-chem-phys.net/8/6469/2008/.

Cooper, D. and Eichinger, W.: Structure of the Atmosphere in an Urban Planetary Boundary Layer From Lidar and Radiosonde Observations, J. Geophys. Res., 99(D11), 22937–22948, 1994.

Cooper, D., Eichinger, W., Leclerc, M. Y., Archuleta, J., and Kao, C. Y. J.: Stable Boundary Layer Coherent Microscale Structures Observed by Lidar, in review, Geophys. Res. Lett., 2010.

CAM: Programa para Mejorar la Calidad del Aire en el Valle de México 2002–2010, Comisión Ambiental Metropolitana, Mexico, 2002.

CAM: Inventario de emisiones de la atmósfera. Zona Metropolitana del Valle de México 2004, Comisión Ambiental Metropolitana, Mexico, 2006.

Davis, K. J., Gamage, N., Hagelberg, C. R., Kiemle, C., Lenschow, D. H., and Sullivan, P. P.: An objective method for deriving atmospheric structure from airborne lidar observations, J. Atmos. Ocean. Tech., 17, 1455–1468, 2000.

DeCarlo, P. F., Dunlea, E. J., Kimmel, J. R., Aiken, A. C., Sueper, D., Crounse, J., Wennberg, P. O., Emmons, L., Shinozuka, Y., Clarke, A., Zhou, J., Tomlinson, J., Collins, D. R., Knapp, D., Weinheimer, A. J., Montzka, D. D., Campos, T., and Jimenez, J. L.: Fast airborne aerosol size and chemistry measurements above Mexico City and Central Mexico during the MILAGRO campaign, Atmos. Chem. Phys., 8, 4027–4048, 2008, http://www.atmos-chem-phys.net/8/4027/2008/.

de Foy, B., Fast, J. D., Paech, S. J., Phillips, D., Walters, J. T., Coulter, R. L., Martin, T. J., Pekour, M. S., Shaw, W. J., Kastendeuch, P. P., Marley, N. A., Retama, A., and Molina, L. T.: Basin-scale wind transport during the MILAGRO field campaign and comparison to climatology using cluster analysis, Atmos. Chem. Phys., 8, 1209–1224, 2008, http://www.atmos-chem-phys.net/8/1209/2008/.

Del Gusta, M. and Marini, S.: On the retrieval of urban mass concentrations by a 532 and 1064 nm LIDAR, J. Aerosol Sci, 31, 1469–1488, 2000.

Di Girolamo, P., Ambrico, P. F., Amodeo, A., Boselli, A., Pappalardo, G., and Spinelli, N.: Aerosol observations by lidar in the nocturnal boundary layer, Appl. Optics, 38, 4585–4595, 1999.

Dillner, A. M., Stein, C., Larson, S. M., and Hitzenberger, R.: Measuring the mass extinction efficiencyof elemental carbon in rural aerosol, Aerosol Sci. Tech., 35, 1009–1021, 2001.

Doran, J. C., Fast, J. D., Barnard, J. C., Laskin, A., Desyaterik, Y., and Gilles, M. K.: Applications of lagrangian dispersion modeling to the analysis of changes in the specific absorption of elemental carbon, Atmos. Chem. Phys., 8, 1377–1389, 2008, http://www.atmos-chem-phys.net/8/1377/2008/.

Dubinsky, R. H., Carswell, A. I., and Pal, S. R.: Determination of cloud microphysical properties by laser backscattering and extinction measurements, Appl. Optics, 24, 1614–1622, 1985.

Dubovik, O., Smirnov, A., Holben, B. N., King, M. D., Kaufman, Y. J., Eck, T. F., and Slutsker, I.: Accuracy assessment of aerosol optical properties retrieval from AERONET sun and sky radiance measurements, J. Geophys. Res., 105, 9791–9806, 2000.

Eichinger, W. E., Holder, H. E., Cooper, D. I., Hipps, L. E., Knight, R., Kustas, W. P., Nichols, J., and Prueger, J. H.: Lidar Measurement of Boundary Layer Evolution to Determine Sensible Heat Fluxes, J. Hydrometeorol., 6, 840–853, 2005.

Eichinger, W. E., Cooper, D. I., Hatfield, J., Hipps, L., Nichols, J. J., Pfeiffer, R., and Prueger, J. H.: Use of Elastic Lidar to Examine the Dynamics of Plume Dispersion from an Agricultural Facility, Atmos. Environ., in review, 2010a.

Eichinger, W., Eichinger, H., Cooper, D., Kreiger, J., and Carlson, E.: Lidar Observations of High Altitude Activity Associated with Intermittent Turbulence in a Stable Atmosphere, Bound. Lay. Meteorol., in review, 2010b.

Eichinger, W. and Kraye, H.: The Use of Lidar to Evaluate Existing

Incident Managment System on I-80 in Morris, Essex, and Passaic Counties in Northern New Jersey, Report No. 980004-7290, New Jersey Department of Transportation, 1998.

Eichinger, W., Buttler, W., Lebeda, C., Cooper, D., and Moses, J.: Barcelona Air Quality Initiative, Alliance for Transportation Research, Project Document ATR 94-1, 1994.

Eichinger, W., Cooper, D., Buttler, W., Cottingame, W., and Tellier, L.: The Use of Lidar for the Evaluation of Traffic-Related Urban Pollution, SPIE Proc, Vol. 2102, Bellingham, WA, 1993.

Eichinger, W., Cooper, D., Cottingame, W., Forman, P., Griegos, J., Osborn, M., Richter, D., Tellier, L., and Thornton, R.: The development of Raman water-vapor and elastic aerosol lidars for the Central Equatorial Pacific Experiment, J. Atmos. Ocean. Tech., 16(11), 1753–1766, 1999.

Emets, E. P., Kascheev, V. A., and Poluektov, P. P.: A New Technique for the Determination of the Density of Airborne Particulate Matter, J. Aerosol Sci., 23(1), 27–35, 1992.

Fast, J. D., de Foy, B., Acevedo Rosas, F., Caetano, E., Carmichael, G., Emmons, L., McKenna, D., Mena, M., Skamarock, W., Tie, X., Coulter, R. L., Barnard, J. C., Wiedinmyer, C., and Madronich, S.: A meteorological overview of the MILAGRO field campaigns, Atmos. Chem. Phys., 7, 2233–2257, 2007, http://www.atmos-chem-phys.net/7/2233/2007/.

Holben, B. N., Eck, T. F., Slutsker, I., Tanré, D., Buis, J. P., Setzer, A., Vermote, E., Reagan, J. A., Kaufman, Y. J., Nakajima, T., Lavenu, F., Jankowiak, I., and Smirnov, A.: AERONET: a federated instrument network and data archive for aerosol characterization, Remote Sens. Environ., 66, 1–16, 1998.

Holmen, B., Eichinger, W., and Flocchini, R.: Application of Elastic Lidar to PM_{10} Emissions from Agricultural NonPoint Sources, Environ. Sci. Technol., 32(20), 3068–3076, 1998.

Husar, R. B. and Falke, S. R.: The relationship between aerosol light scattering and fine mass, Center for Air Pollution Impact and Trend Analysis (CAPITA) Report, online available at: http://capita.wustl.edu/CAPITA/CapitaReports/BScatFMRelation/BSCATFM.HTML, 1996.

Kelly, W. P. and McMurry, P. H.: Measurement of Particle Density by Inertial Classification of Differential Mobility Analyzer Generated Monodisperse Aerosols, Aerosol Sci. Techn., 17(3), 199–212, 1992.

Kleinman, L. I., Springston, S. R., Daum, P. H., Lee, Y.-N., Nunnermacker, L. J., Senum, G. I., Wang, J., Weinstein-Lloyd, J., Alexander, M. L., Hubbe, J., Ortega, J., Canagaratna, M. R., and Jayne, J.: The time evolution of aerosol composition over the Mexico City plateau, Atmos. Chem. Phys., 8, 1559–1575, 2008, http://www.atmos-chem-phys.net/8/1559/2008/.

Kleinman, L. I., Springston, S. R., Wang, J., Daum, P. H., Lee, Y.-N., Nunnermacker, L. J., Senum, G. I., Weinstein-Lloyd, J., Alexander, M. L., Hubbe, J., Ortega, J., Zaveri, R. A., Canagaratna, M. R., and Jayne, J.: The time evolution of aerosol size distribution over the Mexico City plateau, Atmos. Chem. Phys., 9, 4261–4278, 2009, http://www.atmos-chem-phys.net/9/4261/2009/.

Klett, J. D.: Stable analytical inversion solution for processing lidar returns, Appl. Optics, 20, 211–220, 1981.

Klett, J. D.: Lidar inversion with variable backscatter/extinction ratios, Appl. Optics, 24, 1638–1643, 1985.

Kovalev, V. A. and Eichinger, W. E.: Elastic Lidar: Theory, Practice and Analysis Methods, Wiley and Sons, New York, 2004.

Kovalev, V. A.: Lidar measurement of the vertical aerosol extinction profiles with range dependent backscatter-to-extinction ratios, Appl. Optics, 32, 6053–6065, 1993.

Kovalev, V. A.: Sensitivity of the lidar equation solution to errors in the aerosol backscatter-to-extinction ratio: Influence of a monotonic change in the aerosol extinction coefficient, Appl. Optics, 34, 3457–3462, 1995.

Kovalev, V. A.: Stable near-end solution of the lidar equation for clear atmospheres, Appl. Optics, 42, 585–591, 2003.

Krichbaumer, W. and Werner, Ch.: Current state-of-the-art of LIDAR inversion methods for atmospheres of arbitrary optical density, Appl. Phys. B, 59, 517–523, 1994.

Lagrosas, N., Kuze, H., Takeuchi, N., Fukagawa, S., Bagtasa, G., Yoshii, Y., Naito, S., and Yabuki, M.: Correlation study between suspended particulate matter and portable automated lidar data, Aerosol Sci., 36, 439–454, 2005.

Le Bronec, E., Renoux, A., Boulaud, D., and Pourprix, M.: Effect of Gravity in Differential Mobility Analysers. A New Method to Determine the Density and Mass of Aerosol Particles, J. Aerosol Sci., 30, 89–103, 1999.

Mallet, M., Roger, J. C., Despiau, S., Dubovik, O., and Putaud, J. P.: Microphysical and optical properties of aerosol particles in urban zone during ESCOMPTE, Atmos. Res., 69, 73–97, 2003.

Mena-Carrasco, M., Carmichael, G. R., Campbell, J. E., Zimmerman, D., Tang, Y., Adhikary, B., D'allura, A., Molina, L. T., Zavala, M., García, A., Flocke, F., Campos, T., Weinheimer, A. J., Shetter, R., Apel, E., Montzka, D. D., Knapp, D. J., and Zheng, W.: Assessing the regional impacts of Mexico City emissions on air quality and chemistry, Atmos. Chem. Phys., 9, 3731–3743, 2009, http://www.atmos-chem-phys.net/9/3731/2009/.

Molina, L. T., Kolb, C. E., de Foy, B., Lamb, B. K., Brune, W. H., Jimenez, J. L., Ramos-Villegas, R., Sarmiento, J., Paramo-Figueroa, V. H., Cardenas, B., Gutierrez-Avedoy, V., and Molina, M. J.: Air quality in North America's most populous city overview of the MCMA-2003 campaign, Atmos. Chem. Phys., 7, 2447–2473, 2007, http://www.atmos-chem-phys.net/7/2447/2007/.

Molina, L. T., Madronich, S., Gaffney, J. S., and Singh, H. B.: Overview of MILAGRO/INTEX-B Campaign, IGAC Newsletter, Issue No. 38, 2–15, April 2008.

Nakajima T., Tonna G., Rao, R.Z., Boi, P., Kaufman, Y., and Holben, B.: Use of sky brightness measurements from ground for remote sensing of particulate polydispersions, Appl. Optics, 35(15), 2672–2686, 1996.

Nunnermacker, L. J., Weinstein-Lloyd, J. B., Hillery, B., Giebel, B., Kleinman, L. I., Springston, S. R., Daum, P. H., Gaffney, J., Marley, N., and Huey, G.: Aircraft and ground-based measurements of hydroperoxides during the 2006 MILAGRO field campaign, Atmos. Chem. Phys., 8, 7619–7636, 2008, http://www.atmos-chem-phys.net/8/7619/2008/.

Rogers, R. R., Hair, J. W., Hostetler, C. A., Ferrare, R. A., Obland, M. D., Cook, A. L., Harper, D. B., Burton, S. P., Shinozuka, Y., McNaughton, C. S., Clarke, A. D., Redemann, J., Russell, P. B., Livingston, J. M., and Kleinman, L. I.: NASA LaRC airborne high spectral resolution lidar aerosol measurements during MILAGRO: observations and validation, Atmos. Chem. Phys., 9, 4811–4826, 2009, http://www.atmos-chem-phys.net/9/4811/2009/.

Shaw, W. J., Pekour, M. S., Coulter, R. L., Martin, T. J., and

Walters, J. T.: The daytime mixing layer observed by radiosonde, profiler, and lidar during MILAGRO, Atmos. Chem. Phys. Discuss., 7, 15025–15065, 2007, http://www.atmos-chem-phys-discuss.net/7/15025/2007/.

Shon, Z.-H., Madronich, S., Song, S.-K., Flocke, F. M., Knapp, D. J., Anderson, R. S., Shetter, R. E., Cantrell, C. A., Hall, S. R., and Tie, X.: Characteristics of the NO-NO_2O_3 system in different chemical regimes during the MIRAGE-Mex field campaign, Atmos. Chem. Phys., 8, 7153–7164, 2008, http://www.atmos-chem-phys.net/8/7153/2008/.

Stephens, S., Madronich, S., Wu, F., Olson, J. B., Ramos, R., Retama, A., and Muñoz, R.: Weekly patterns of Mxico City's surface concentrations of CO, NO_x, PM_{10} and O_3 during 1986–2007, Atmos. Chem. Phys., 8, 5313–5325, 2008, http://www.atmos-chem-phys.net/8/5313/2008/.

Stone, E. A., Snyder, D. C., Sheesley, R. J., Sullivan, A. P., Weber, R. J., and Schauer, J. J.: Source apportionment of fine organic aerosol in Mexico City during the MILAGRO experiment 2006, Atmos. Chem. Phys., 8, 1249–1259, 2008, http://www.atmos-chem-phys.net/8/1249/2008/.

Talbot, R., Mao, H., Scheuer, E., Dibb, J., Avery, M., Browell, E., Sachse, G., Vay, S., Blake, D., Huey, G., and Fuelberg, H.: Factors influencing the large-scale distribution of Hg° in the Mexico City area and over the North Pacific, Atmos. Chem. Phys., 8, 2103–2114, 2008, http://www.atmos-chem-phys.net/8/2103/2008/.

Tang, I.: Chemical and size effects of hygroscopic aerosols on light scattering coefficients, J. Geophys. Res., 101, 19245–19250, 1996.

Thornhill, D. A., de Foy, B., Herndon, S. C., Onasch, T. B., Wood, E. C., Zavala, M., Molina, L. T., Gaffney, J. S., Marley, N. A., and Marr, L. C.: Spatial and temporal variability of particulate polycyclic aromatic hydrocarbons in Mexico City, Atmos. Chem. Phys., 8, 3093–3105, 2008, http://www.atmos-chem-phys.net/8/3093/2008/.

van de Hulst, H.C.: Light Scattering by Small Particles, Wiley and Sons, New York, 1957.

Zheng, J., Zhang, R., Fortner, E. C., Volkamer, R. M., Molina, L., Aiken, A. C., Jimenez, J. L., Gaeggeler, K., Dommen, J., Dusanter, S., Stevens, P. S., and Tie, X.: Measurements of HNO_3 and N_2O_5 using ion drift-chemical ionization mass spectrometry during the MILAGRO/MCMA-2006 campaign, Atmos. Chem. Phys., 8, 6823–6838, 2008, http://www.atmos-chem-phys.net/8/6823/2008/.